

Computational study of antiferromagnetic and mixed-valent diamagnetic phase of AgF₂: crystal, electronic and phonon structure and p-T phase diagram

Kamil Tokár,^{a;b} Mariana Derzsi,^{a;c} and Wojciech Grochala^c

Crystal and electronic structure, lattice dynamics and thermodynamic stability of little known mixed-valent diamagnetic Ag¹⁺Ag³⁺F₄ β form of AgF₂ is thoroughly examined for the first time and compared with well known antiferromagnetic Ag²⁺F₂ α form within the framework of Density Functional Theory based methods, phonon direct method and quasiharmonic approximation. Computed equations of state, bulk moduli, electronic densities of states, electronic and phonon band structures including analysis of optically active modes and p-T phase diagram of the α - β system are presented. This study demonstrates that α is thermodynamically preferred over β at all temperatures and pressures of its existence but simultaneously β is dynamically stable in much broader pressure range. The β phase is discussed in broader context of isostructural ternary metal fluorides and isoelectronic oxides including NaCuO₂ – the reference compound for existence of Cu³⁺ species in high-temperature oxocuprate superconductors.

1 Introduction

Two polymorphic forms have been reported for AgF₂ at ambient conditions – layered antiferromagnetic (α) and diamagnetic (β). The α phase exhibits numerous structural and electronic similarities with oxocuprate precursors of high-temperature superconductors, including the 2D antiferromagnetic (AFM) AgF₂ sheets with large AFM super-exchange constant that have the same topology as [CuO₂] layers that mediate superconductivity in the high-temperature superconducting oxocuprates.¹ Physico-chemical properties of the α phase including crystal and magnetic structure^{2–4}, electronic structure,^{1,5} and high-pressure polymorphism^{6–9} have been thoroughly scrutinized and α phase is a subject of many of our ongoing studies. On the other hand, the β phase is much less understood. It has been obtained as a red-brown diamagnetic product of reaction of AgBF₄ with KAgF₄ in anhydrous HF and magnetic measurements suggested mixed-

valent Ag¹⁺Ag³⁺F₄ system.¹⁰ Although its crystal structure could not be determined due to the lack of crystallinity it is assumed to take KBrF₄ structure type, which is typical for Ag¹⁺Au³⁺F₄ and other ternary metal fluorides M'MF₄ with coinage (M) and alkali metals (M').^{10–12} Notably, the β phase undergoes a rapid exothermic conversion to the α form accompanied with charge transfer Ag¹⁺Ag³⁺F₄ \rightarrow 2Ag²⁺F₂ when the temperature is raised from -80 C to 0 C. This behaviour can be contrasted with charge-transfer instability in oxocuprates. Some authors suggest that charge-transfer instability of the parent insulating cuprates may drive their unconventional superconductivity.¹³ A direct relation between unconventional superconductivity and the disproportionation reaction is well documented for charge-ordered insulator BaBi^{3+/5+}O₃, which can be converted to a superconductor by a nonisovalent substitution Ba_{1-x}K_xBiO₃. However, the charge ordered Cu¹⁺/Cu³⁺ form has never been observed in undoped oxocuprates. Instead, NaCuO₂ has been studied as reference compound for the existence of Cu³⁺ species in high-temperature oxocuprate superconductors.^{14–16} On the other hand, its silver counterpart in form of Ag¹⁺Ag³⁺O₂ is known but in this case the comproportionated Ag²⁺O has never been observed.^{17–22} Instead it exists in two disproportionated polymorphic forms, monoclinic¹⁷ and tetragonal,¹⁸ and remains mixed-valent semiconductor up to extremely high pressures (75 GPa).²³ Thus, the appearance of both the comproportionated Ag²⁺ and disproportionated Ag^{1+/3+} states in AgF₂ renders this system unique and requires detailed examination.

^a Advanced Technologies Research Institute, Faculty of Materials Science and Technology in Trnava, Slovak University of Technology in Bratislava, J. Bottu 25, 917 24 Trnava, Slovakia. E-mail: mariana.derzsi@stuba.sk

^b Institute of Physics, Slovak Academy of Sciences, Dúbravská cesta 9, 845 11 Bratislava, Slovakia.

^c Center of New Technologies, University of Warsaw, Zwirki i Wigury 93, 02089 Warsaw, Poland.

Crystal structure and stability of the β relative to the α AgF₂ were first addressed in a theoretical Density Functional Theory (DFT) study dedicated to pressure-induced transformations of AgF₂.⁶ The study revealed metastability of the β over α by +0.17 eV per one AgF₂ unit at ambient conditions and growing further with increasing pressure. However, only results of total energy calculations were presented while the impact of lattice dynamics and temperature have remained open questions; the former was later demonstrated to have crucial impact on high-pressure phase transitions in the α phase.^{8,9} The study also did not consider the strong electron correlations and magnetism, which are important for proper description of AgF₂ system.^{1,4,5,8,9} It is also not known if the KBrF₄ type candidate for the β phase is dynamically stable and if so, what is the character of its electronic structure and how do the crystal, electronic and phonon structure evolve with pressure. Considering the α phase, although it is much better understood, its lattice dynamics has not been analyzed in detail before and impact of temperature on its stability is also unknown. In this work, we address all the above issues in a computational study from the perspective of DFT-based methods, phonon direct method and quasiharmonic approximation while accounting for strong electron correlations and magnetism.

Here we present results of a detailed comparative computational DFT+U study of crystal and electronic structure and lattice dynamics of the α and the β AgF₂ phase (with larger focus on the less known β , considering the KBrF₄ structure type) and a theoretical p - T phase diagram of the α β system. The crystal, electronic and phonon structure of both phases are compared also as functions of pressure and pressure-dependences of their Raman and IR active frequencies are provided. Furthermore, we discuss the electronic structure of both phases from the perspective of DFT+U and hybrid DFT method since the latter is known to provide more realistic values for the insulating band gaps.²⁴ Finally, all our results obtained for the β phase are confronted with available literature data for isostructural fluorides M'MF₄ with coinage (M) and alkali metals (M') and with isoelectronic NaCu³⁺O₂ and Ag¹⁺Ag³⁺O₂.

2 Calculation details

Periodic DFT calculations for the α and β phase of AgF₂ were performed in the plane-wave VASP program with PAW-GGA method,^{25,26} PBEsol functional,²⁷ plane-wave cut-off energy set to 520 eV and k -mesh spacing of 0.28 Å⁻¹ for cell relaxation and 0.14 Å⁻¹ for electronic structure calculations. The onsite electron correlations on Ag d orbitals were accounted for using the rotationally invariant DFT+U method introduced by Liechtenstein *et al.*, where the values of both Hubbard U and the Hund J parameter are set explicitly²⁸. We have used the values $U_{Ag} = 5$ eV and $J_{Ag} = 1$ eV in accordance with the previous studies.^{4,8,9} In case of the α phase, spin-polarized calculations were performed considering the known AFM ground-state.²⁻⁴ Electronic density of states and band structure were further recalculated for the DFT+U optimized structures with hybrid HSE06 functional with 25% of exact exchange.²⁹ Phonon dispersion curves and phonon density of states (PDOS) were calculated with direct phonon method in the pressure interval ranging from -6 GPa to

+8 GPa (at higher pressures the α phase transforms to a ferroelectric Pca2₁ form⁸). These calculations were performed for 2 x 2 x 2 (a) and 2 x 2 x 1 (b) supercells (96 atoms each), with the reciprocal space sampled over the 4 x 4 x 4 Monkhorst-Pack k -mesh.³⁰ The pressure dependent PDOSes were subsequently used to obtain thermodynamic functions within quasi-harmonic approximation (QHA). The phonon and thermodynamics calculations were performed in program PHONOPY.³¹ The force constants were derived from Hellmann-Feynman forces that were computed with finite atomic displacement equal to 0.02 Å at DFT+U level. Dynamical matrices were constructed considering full symmetries of the supercell. The equation of state obtained in QHA approximation enables for estimation of thermoelastic properties. The α β phase diagram was constructed from the Gibbs energy isobars in the p - T diagram. Thermodynamic potentials of both crystalline phases were derived from the free energy $F_{\text{phon}}(T, V)$ of calculated phonon system and ground state energies of the phases at given external pressure p and temperature T within QHA. Phase relations between α and β phases and their relative thermodynamic stability were constrained from Gibbs energy isobars by determining the boundary locus of points in p - T phase diagram, where crystal structures of the two phases satisfy Gibbs rule of thermal equilibrium $G^{\alpha}(T, p) = G^{\beta}(T, p)$.

3 Results

3.1 Crystal structure

Crystal structures of α and β AgF₂ are shown in Figure 1.

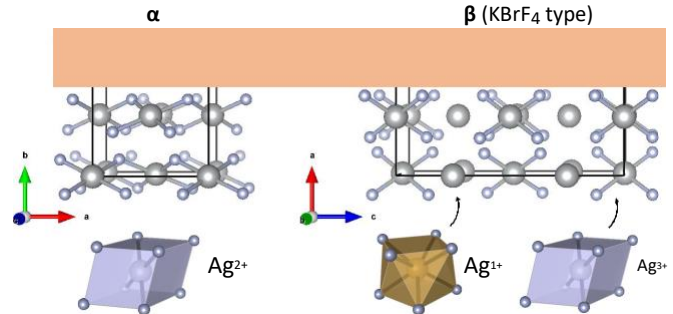


Fig. 1 Comparison of crystal structure of α and β AgF₂ and their extended Ag coordination polyhedra: (left) experimental orthorhombic α with Pnma symmetry and (right) hypothetical tetragonal β assuming KAgF₄ I4/mcm structure type. Note, β can be viewed as a structure, where every other Ag²⁺ F bond within each AgF₂ layer (highlighted with orange stripe) has been broken. The bonds within the coordination polyhedra indicate the first coordination sphere.

The α phase crystallizes in orthorhombic Pnma symmetry with neutral AgF₂ layers stacked in ABAB fashion along b crystallographic axes. Coordination of the Ag²⁺ ions within the layers is square planar [AgF₄]. The first nearest-neighbour axial F contacts complete elongated octahedral coordination and the second nearest-neighbour ones complete deformed rhombic prism (2+2+2+2 coordination). The structure was thoroughly characterized before.² Our DFT+U calculations reproduce very well all experimental structural parameters including Ag F distances

Table 1 Selected structural data for α - and β -AgF₂ and for A¹⁺Ag³⁺F₄ and A¹⁺Au³⁺F₄ compounds (where A stands for alkali metal) with KBrF₄ type structure. DFT+U values were computed in this work and experimental values are taken from literature.

Struc.	Ref.	V/AgF ₂	a	b	c	M ²⁺ -F _{eq}	M ²⁺ -F _{ax}	M ³⁺ -F _{eq}	M ³⁺ -F _{ax}	Ag ¹⁺ -F	F-Ag ³⁺ -F	F-Ag ¹⁺ -F
a-AgF ₂	exp ²	40.8	5.529	5.813	5.073	2.067, 2.071	2.588					
a-AgF ₂	DFT+U	40.5	5.498	5.824	5.055	2.069, 2.071	2.568					
b-AgF ₂	DFT+U	40.8	5.524		10.704			1.933	2.848	2.432	92.2	113.4
NaAgF ₄	exp ³²	40.5	5.540		10.560			1.896	2.906	2.430	89.9	115.4
AgAuF ₄	exp ³³	45.4	5.791		10.817			1.885	3.016	2.577	93.3	113.6
KAgF ₄	exp ³²	48.5	5.900		11.150			1.896	3.129	2.646	90.2	113.6
KAuF ₄	exp ³⁴	51.0	5.990		11.380			1.998	3.154	2.652	90.1	114.5
RbAuF ₄	exp ³²	56.6	6.180		11.850			1.998	3.273	2.788	90.2	112.3

(the short square-planar distances within 0.001 Å, the longer axial contacts within 0.02 Å) and unit cell volumes (within less than 1%) (Table 1).

In β phase with tetragonal KBrF₄ structure two non-equivalent Ag ions are present, square planar and square antiprismatic one organized into separate layers alternating along the tetragonal c direction (Figure 1). The [AgF₄] square plaquettes are isolated from each other, oriented perpendicular to the ab layers and to each other in all three crystallographic directions. The calculated Ag F distances of the square-planar silver (1.933 Å) are noticeably shorter relative to the corresponding distances in α (2.069 and 2.071 Å). This is in line with slightly smaller Ag³⁺ ion in respect to Ag²⁺ and indeed the values follow closely those expected based on tabulated ionic radii by Shannon, ³⁵ Ag³⁺ F (1.98 Å) and Ag²⁺ F (2.1 Å) ones. The square-planar silver in β has additionally four secondary axial contacts equal to 2.848 Å that complete its coordination to distorted rhombic prism. This contrasts with much shorter axial contacts equal to 2.568 Å that complete the octahedral coordination of Ag²⁺ in α . The longer secondary contacts in b reflect the tendency of Ag³⁺ to avoid mutual secondary interactions Ag³⁺F...Ag³⁺. From this point of view, KBrF₄ type structure is an ideal host for Ag³⁺ since it effectively minimizes the mutual secondary Ag³⁺F...Ag³⁺ interactions by allowing for perfect antiferrodistortive ordering of the [Ag³⁺F₄] plaquettes in all three crystallographic directions. The square antiprismatic silver has eight equivalent Ag F distances equal to 2.432 Å. This value is slightly shorter than the one observed for Ag¹⁺ in isostructural Ag¹⁺Au³⁺F₄ (2.577 Å), ³³ which in turn is very close to the value based on the tabulated ionic radius for 8-coordinated Ag¹⁺ (2.59 Å). On the other hand, it is almost identical to the Na⁺ F distance (2.43 Å) in isostructural Na¹⁺Ag³⁺F₄. ³² In fact, all structural parameters calculated for the β phase follow very closely those of NaAgF₄ including almost identical volumes of 326.7 (Ag¹⁺) and 324.1 (Na¹⁺) and primary/secondary Ag³⁺ F contacts of 1.933 Å /2.848 Å (in Ag¹⁺Ag³⁺F₄) and 1.896 Å /2.906 Å (in Na¹⁺Ag³⁺F₄). These results are in line with the well-known similarities between Ag¹⁺ and Na¹⁺. Comparison with other isostructural compounds containing Ag³⁺ and Au³⁺ species may be observed in Table 1.

Despite the above described differences between α and β form, their crystal structures are intimately related. Both share the same fluorite metal sublattice and differ only in different displacements of the fluorine atoms. In case of the β phase, the displacements of F atoms lead to doubling of the fluorite unit cell along the c

axis. Also note, that one can rationalize the β phase as the α phase with bond-broken AgF₂ layers (Figure 1). The breaking of the Ag-F bonds takes place due to charge disproportionation Ag²⁺Ag²⁺! Ag¹⁺Ag³⁺ and leads to doubling of the a lattice vector of α (Figure 1). It should be noted that in the fluorite structure, the metal cations are in cubic coordination with the ligands. In the α phase, the extended coordination of silver cations is in first approximation angularly deformed cubic (rhomboid), while the orthorhombic symmetry drives the coordination to an elongated octahedron. In the β phase, half of the coordination polyhedra belonging to Ag³⁺ are deformed rhomboids and another half (Ag¹⁺) are square antiprisms or in another words twisted cubes. In fact, both structures are related to the fluorite structure by group-subgroup relation involving in each case single order

parameter X5+, resp. L3+/L3-: Fm-3m (fluorite)! X5+ Pbcu (a) and Fm-3m (fluorite)! L3+(L3-) I4/mcm (b) and thus could be understood as emerging from the fluorite structure via a distinct ordering parameter. The group-subgroup analysis was performed using ISOTROPY Software Suite. ³⁶

Quite remarkably, the computed volumes per one AgF₂ unit of α and β are extremely similar. The calculated unit cell volumes at zero external pressure are V_a = 161.86 Å³ and V_b = 326.66 Å³ (they contain 4 and 8 AgF₂ units per unit cell, respectively). These translate to 40.47 Å³ and 40.83 Å³ per one AgF₂ unit, respectively; β having less than 1% larger volume. Interestingly, this relationship holds also under pressure at least up to 10 GPa (Figure 2). Around this pressure, the α form transforms to a non-centrosymmetric Pca21 structure. ⁸ Similar compressibility of the two forms translates to bulk modulus of b (B₀ = 54 GPa) being only slightly larger than bulk modulus of a (B₀ = 50 GPa). Interestingly, compressibility of both forms is comparable despite their entirely different electronic character as discussed in Section 3.2. It is simultaneously much higher when compared to other electronically and structurally related compounds. For example, CuF₂, which is the lighter counterpart of a-AgF₂ is considerably less compressible with DFT+U bulk modulus equal to 75 GPa. ³⁷ Additionally, when computed in α -AgF₂ structure type, its bulk modulus amounts to 71 GPa. ³⁷ Since both, CuF₂ and α -AgF₂ are isoelectronic and their crystal structures differ only in stacking of otherwise similar puckered metal fluoride layers, the larger compressibility of a-AgF₂ is related to presence of larger (and softer) Ag²⁺ cation relative to Cu²⁺. In case of β -AgF₂, neither its lighter nor heavier counterpart exists. The only isoelectronic compound with known compressibility is Ag¹⁺Ag³⁺O₂. Its bulk modulus es-

timated from high-pressure X-ray diffraction and DFT+U data is even higher close to 83 GPa.²³ However, its crystal as well as electronic structure differ from β -AgF₂ as discussed in Section 3.5.

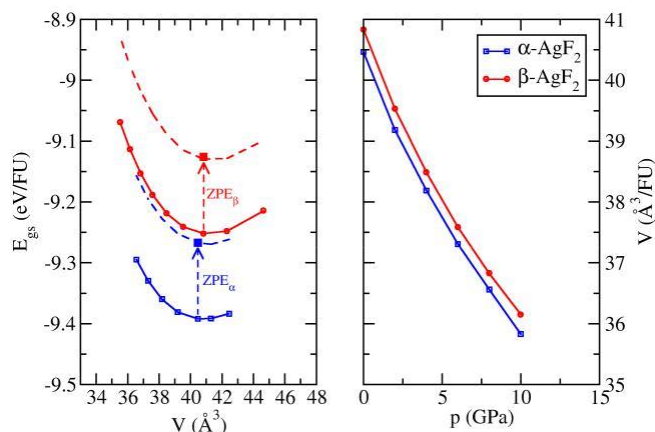


Fig. 2 Equation of state for α - and β -AgF₂ for T=0 K (DFT+U re-sults). The left panel depicts the static energy dependence on volume per one AgF₂ unit (continuous curves) together with ZPE correction (dashed curves) plotted with a 3rd-order polynomial fit. The energy minima correspond to zero external pressure. The right panel depicts p-V dependence.

The β phase is the most compressible within the tetragonal plane. At 8 GPa the a and c lattice vectors reduce to 95.6% and 98.4% of their zero-pressure values, respectively. The higher compressibility within the tetragonal plane is governed by the four axial Ag³⁺F...F contacts. They are the longest and the most compressible contacts in the structure running along the ab plain diagonal. At 8 GPa, they experience reduction by 0.13 Å from 2.848 Å to 2.719 Å. Second in line are the eight square antiprismatic Ag¹⁺F contacts that reduce by 0.082 Å from 2.432 Å to 2.331 Å. The least compressible or the most rigid ones are the square planar Ag³⁺F bonds. They reduce only by 0.004 Å from 1.933 Å to 1.927 Å. Even at pressure of 20 GPa, the length of these bonds is reduced by no more than 0.018 Å in contrast with 0.224 Å and 0.373 Å reduction for the Ag¹⁺F and Ag³⁺F...F respectively, which further manifests the rigidity of the former bonds.

The rigidity of the square-planar Ag³⁺F bonds is comparable to that of the square-planar Ag²⁺F bonds in the α phase. The latter was previously examined in a combined high-pressure XRD and DFT study.⁸ The lattice parameters of α and β computed in function of pressure are compared in Table S1 in ESI.

It is interesting to observe evolution of the tetragonal c/a ratio of the β phase under pressure and confront it with the range of c/a ratios observed in related compounds with KBrF₄ structure congaing coinage metals. The c/a ratio of the β phase at zero pressure is 1.94 and it increases with pressure. For Ag³⁺ and Au³⁺ compounds this ratio is found within the range 1.87 – 1.92,^{12,32–34} while the highest value of 2.06 is observed for CsCu³⁺F₄.³⁸ This seems to be the limiting case, since LiAuF₄ and CsAuF₄ with higher c/a ratios of 2.07 and 2.10 crystallize in mon-

oclinic and orthorhombic variant of KBrF₄ structure, respectively. According to our DFT+U results, b phase would reach this value at pressures above 20 GPa. This result can be confronted with our phonon calculations (discussed below), which indicate dynamical stability at least up to 20 GPa, the highest calculated pressure. Interestingly, KBrF₄ type compounds containing Ag²⁺ in combination with divalent cations such as Ca²⁺, Sr²⁺, Ba²⁺, Zn²⁺, Cd²⁺ and Hg²⁺ instead of K⁺ are also known and their c/a ratios are observed within the range 1.9 – 1.99.³⁹ Note, this ratio is slightly higher than for the KBrF₄ type compounds with Ag³⁺ (1.89 for NaAgF₄ and 1.91 for KAgF₄). In β , the highest of these two values is reached at 8 GPa. This observation alone suggests that b phase has the potential to accommodate also Ag²⁺ in a wide pressure interval. Since the KBrF₄ type compounds with Ag²⁺ are paramagnetic,³⁹ we have tried to reach magnetic solutions for the β phase at all calculated pressures. However, our attempts to stabilize antiferromagnetic solutions for β were unsuccessful and ferromagnetic solution was found higher in energy in respect to diamagnetic at all pressures.

3.2 Electronic structure

Electronic structures of α and β -AgF₂ are presented in Figure 3 (electronic DOS) and Figure 4 (electronic band structure).

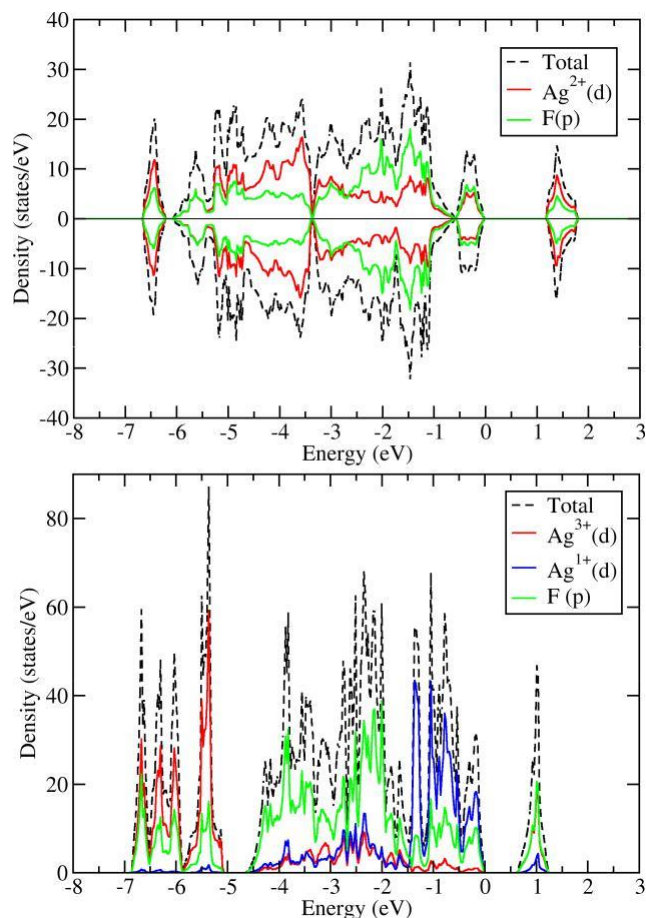


Fig. 3 Electronic DOS of antiferromagnetic α (top) and diamagnetic β AgF₂ (bottom) calculated with DFT+U.

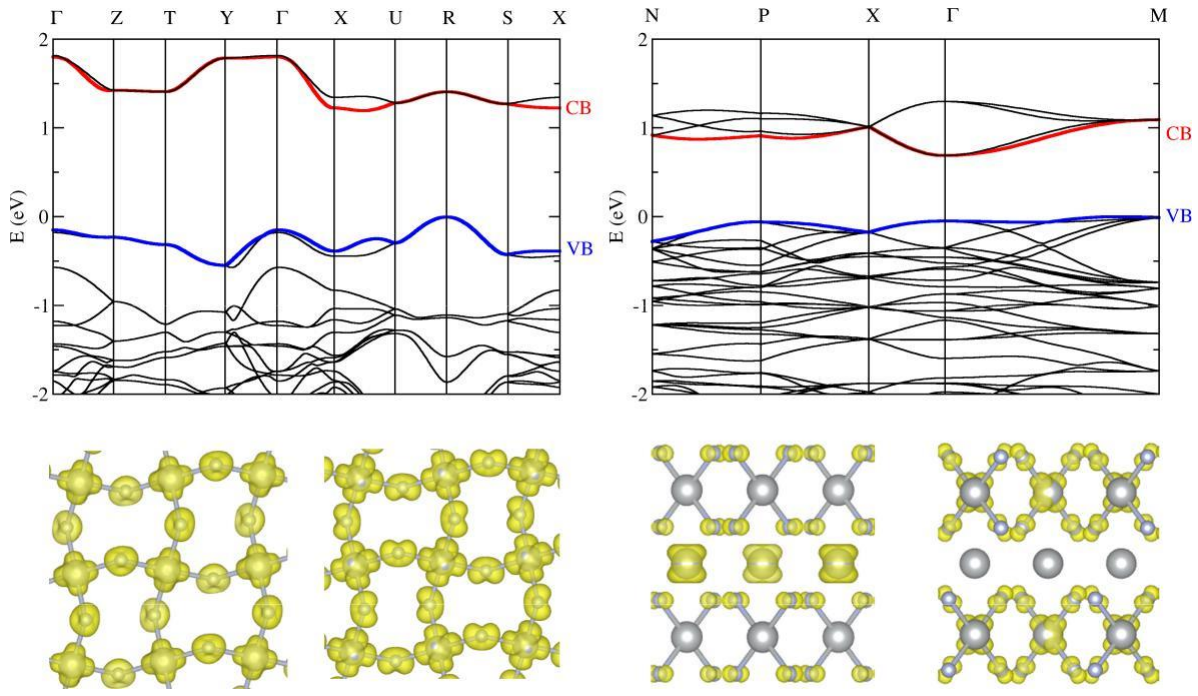


Fig. 4 Electronic band structure (BS, top) and real-space projection of the valence band (VB, blue curve in the BS) and the conduction band (CB, red curve in the BS) (bottom) of α - (left) and β -AgF₂ (right) calculated with DFT+U.

Electronic density state (eDOS) of α -AgF₂ projected on individual atoms reveal strong mixing of Ag and F states across the entire 7 eV wide valence region (Figure 3, top). The large overlap of Ag and F states is a consequence of the extended 2D network of short Ag-F bonds. The highly localized covalent character of the Ag-F bonds is witnessed by the narrow peaks positioned at the very bottom and very top of the valence DOS. The bonds form between the Ag $d(x^2 - y^2)$ and F $p(x)/p(y)$ orbitals. The bottom peak centered at 6.5 eV corresponds to the respective s bonding states of prevalent Ag $d(x^2 - y^2)$ character (the lower Hubbard band) and the top one centered at 0.25 eV to s antibonding of predominant F p character. An insulating bandgap of 1.17 eV opens between the s antibonding states and upper Hubbard band of predominant Ag $d(x^2 - y^2)$ character as expected for formally Ag²⁺ cation with d^9 electronic configuration and a hole in the e_g states. The real-space (orbital) projections of these bands reveal contribution from the $p(z)$ states to the valence band but not to the conduction band (Figure 4, bottom left). Electronic band structure calculations reveal formation of indirect insulating bandgap along R – X direction in the Brillouin zone. (Figure 4, top left) These results show that α -AgF₂ is a charge-transfer indirect bandgap insulator in agreement with our previous studies.^{1,5} Very similar electronic structure is observed in undoped cuprates, which makes AgF₂ an excellent cuprate analogue.¹

A distinct picture of electronic structure is obtained for β -AgF₂. Here, the eDOS projected on individual atoms reveal distinct contribution from the square-planar and the square-antiprismatic silver atom (Figure 3, bottom). The d states of the former are found predominantly in the bottom of the valence DOS and the d states of the latter silver are dominantly located in the upper parts of the valence DOS. In case of the square-antiprismatic silver, all d

states are occupied as expected for closed shell d^{10} Ag¹⁺ cation. On the other hand, the s antibonding $d(x^2 - y^2)$ states are depopulated in case of the square-planar silver in line with low spin d^8 configuration characteristic for Ag³⁺ species involved in a covalent bond. The s bonding Ag³⁺ states are found at the very bottom of the valence DOS centered at 6.7 eV. However, the energy separation of the s bonding and s antibonding states is larger in β ($\Delta\sigma - \sigma^* = 7.6$ eV) by 1.3 eV, which confirms presence of even stronger covalent bonds in comparison to a ($\Delta\sigma - \sigma^* = 6.25$ eV). Furthermore, all Ag³⁺ d states are much more localized compared to Ag²⁺ d states in a. They form highly localized bands within narrow 3 eV-wide range between 7 and 5 eV separated from remaining valence DOS by a bandgap of 0.5 eV in contrast to Ag²⁺ d states in a, which overlap with F p states across the entire valence DOS. The high localization of the Ag³⁺ d states in b shows that they are not involved in formation of extended bonding network in contrary to corner-sharing [Ag²⁺F₄] plaquettes in a. Instead, they are confined to the co-valent bonds within the isolated [Ag³⁺F₄] plaquettes held in the crystal by electrostatic interactions with Ag¹⁺ cations. Presence of typical Ag¹⁺-F bonds in β -AgF₂ is witnessed by highly localized character of the valence Ag¹⁺ states positioned on top of the valence F bands. A bandgap of 0.62 eV opens between the nonbonding Ag¹⁺ states and σ antibonding Ag³⁺ states (Ag¹⁺

→ Ag³⁺ inter-valence charge-transfer) between M and G point of the Brillouin zone (Figure 4, top right). The real-space projections of the highest occupied and the lowest unoccupied states show that the former is constructed from Ag¹⁺ $d(xz)$, $d(yz)$ and F $p(z)$ atomic orbitals whereas the latter involves Ag³⁺ $d(x^2 - y^2)$, F $p(x)$ and $p(y)$ (Figure 4, bottom right). Thus, β -AgF₂ is a distinct charge-transfer insulator with the insulating bandgap by factor of

2 smaller compared to the insulating bandgap of the α phase.

Under compression, electronic structure of both AgF₂ phases does not change significantly within the pressure range of their dynamical stability. Both experience typical broadening of all electronic bands with increasing pressure. However, in case of the β phase, slow progress towards increased hybridization of all Ag d and F p states with the pressure (reminiscent of the α phase) is evident. Evolution of electronic DOS with pressure can be observed for both AgF₂ phases in Figures S2 and S3 in ESI. The band gaps of both phases decrease under compression while the band gap of α remains broader and both phases remain insulating at all calculated pressures. We have recalculated the band gaps also with hybrid DFT, which is known to provide a better estimate for insulating bandgaps. These calculations provide the zero-pressure value of 2.34 eV for α and 1.17 eV for β and so by factor of 2 wider bandgaps in respect to DFT+U. However, also on hybrid DFT level the bandgap of β is by factor of 2 smaller relative to α and retains its insulating character at all calculated pressures (Table 2). Similar DFT+U and hybrid DFT values of the band gap were obtained for the α phase in previous studies.^{1,4,5} For completeness, evolution of electronic DOS calculated for α and β phase with hybrid DFT can be observed in Figures S4 and S5 in ESI. Similar picture is obtained as with DFT+U method including large overlap between Ag²⁺ d and F p states for α and large localization of the Ag³⁺ and Ag¹⁺ d at the bottom and top of the valence region for β . Additionally, Hybrid DFT points out to a larger mixing of the F p states with the Ag³⁺ d and a smaller overlap with the Ag¹⁺ d states relative to DFT+U picture.

Table 2 Evolution of insulating bandgap with pressure calculated for the α - and β -AgF₂ on DFT+U and hybrid DFT (HSE06) level.

p(GPa)	E _{gap} ^a		E _{gap} ^b	
	DFT+U	HSE06	DFT+U	HSE06
0	1.169	2.341	0.613	1.171
2	1.141	2.289	0.501	1.050
4	1.111	2.261	0.426	0.987
6	1.098	2.251	0.367	0.903
8	1.104	2.220	0.308	0.841

3.3 Lattice dynamics

The phonon dispersion curves and phonon density of states (PDOS) of the α and β phase integrated over entire Brillouin zone are shown jointly in Figure 5. Comparing first the phonon dispersion curves, one can immediately notice large difference in lattice dynamics between the two phases. In the β phase they cover broader frequency range 0–590 cm⁻¹ in contrast to 0–500 cm⁻¹ in α . Furthermore, the phonon bands of α are much more dispersed and coupled than those in the β phase.

In α , the phonons are split to two energy regions separated at around 200 cm⁻¹ by a 25 cm⁻¹ wide gap (Figure 5, top). The PDOS reveals that the higher energy region is dominated by contributions from F atoms, while Ag atoms contribute considerably to the bands in the range 0–200 cm⁻¹ and dominate the phonon spectrum below 100 cm⁻¹. The most dispersed bands are found in the higher energy region that covers the bond stretching and bending vibrations. The high dispersion of these bands results in

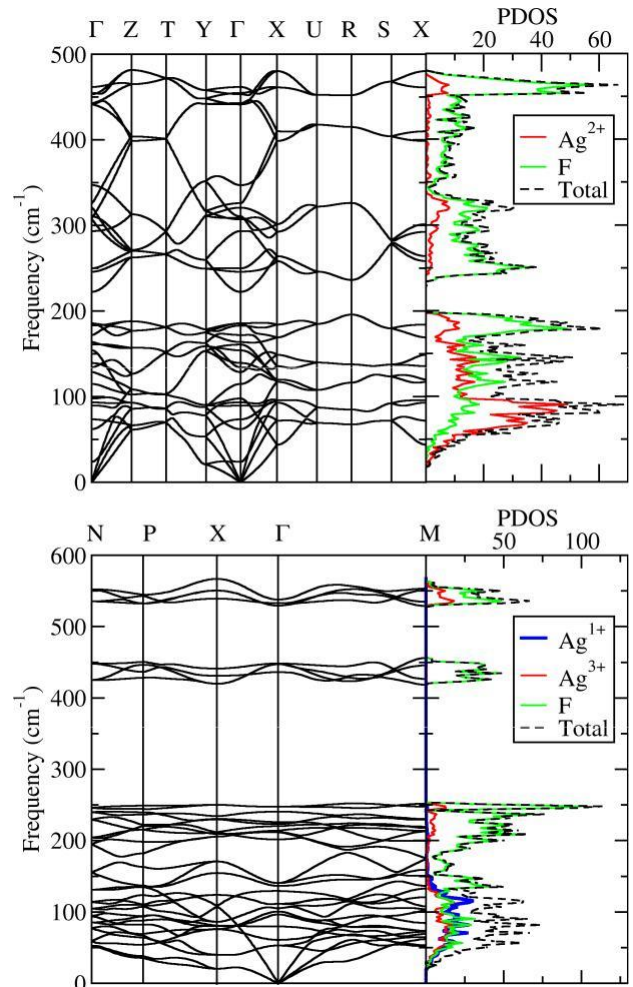


Fig. 5 Calculated phonon dispersion curves and phonon density of states of α - (top) and β -AgF₂ (bottom). DFT+U results.

their strong coupling and consequently in appearance of one continuous energy region between 225 and 500 cm⁻¹. In β , on the other hand, the high-energy stretching modes are localized into two very narrow energy regions less than 50 cm⁻¹ wide. They are centred at 440 and 540 cm⁻¹, and belong to symmetric and asymmetric bond stretching vibrations within [AgF₄] units, respectively. They are completely separated from each other by cca. 80 cm⁻¹ wide phonon bandgap as well as from the lower-energy region by 180 cm⁻¹ wide bandgap. The lower-energy region spreads over the energy range 0–250 cm⁻¹. The PDOS reveals that the phonon spectrum of β is dominated by the contributions from fluorine atoms similarly as in α . On the other hand, noticeable differences can be observed in redistribution of the silver phonon states that is additionally related to presence of two distinct silver atoms. The square planar Ag³⁺ silver contributes to all but the bands centered around 430 cm⁻¹, while the square antiprismatic Ag¹⁺ silver contributes only to the lowest energy bands below 150 cm⁻¹. The large separation of the symmetric and asymmetric [Ag³⁺F₄] stretching vibrations (D = 80 cm⁻¹) contrasts with the situation in the α phase, where the respective [Ag²⁺F₄] vibrations are only cca. 10 cm⁻¹ apart and centered around 450 cm⁻¹. The Γ -point centered asymmetric [Ag³⁺F₄]

stretching vibrations appear at much higher energies (530–540 cm^{-1}) in respect to the asymmetric $[\text{Ag}^{2+}\text{F}_4]$ ones in a (450–460 cm^{-1}). On the other hand, the symmetric $[\text{Ag}^{3+}\text{F}_4]$ stretching vibrations appear at only slightly higher energies (447–450 cm^{-1}) in respect to the symmetric $[\text{Ag}^{2+}\text{F}_4]$ ones (440–445 cm^{-1}). The overall higher $\text{Ag}^{3+}\text{-F}$ stretching frequencies are in line with formation of stronger covalent bonds in the β phase. Also, contribution of the square antiprismatic silver only to the lowest energy bands is in line with formation of closed shell Ag^{1+} cation. The above described features of lattice dynamics of α and β phase manifest presence of chemically and electronically distinct lattices. Highly localized dispersionless bands in β manifest the presence of the electronically isolated $[\text{Ag}^{3+}\text{F}_4]$ plaquettes and thus the lack of extended crystal network of covalent bonds. On the other hand, the highly dispersed and strongly coupled phonon bands in α manifest presence of the extended network of covalent $\text{Ag}^{2+}\text{-F}$ bonds. One can observe that the largest dispersion of the bands in α takes place mostly along the $\Gamma\text{-X}$, $\Gamma\text{-Y}$, $\Gamma\text{-Z}$ and

T-Y directions in the 1st Brillouin zone.

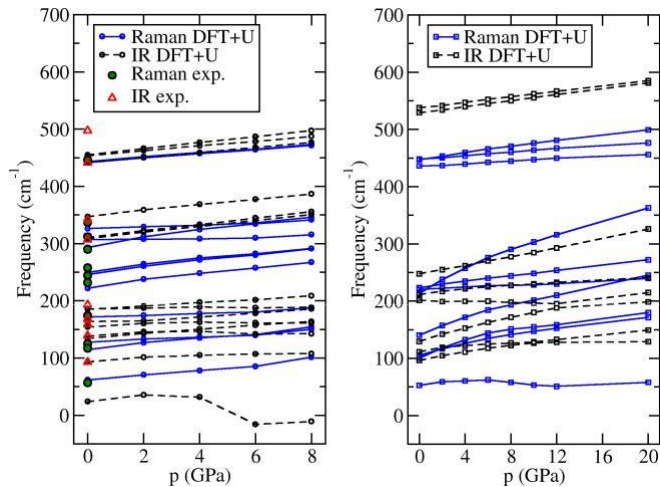


Fig. 6 Pressure-dependence of Raman and IR active frequencies calculated for α (left) and β (right) AgF_2 phase. DFT+U results.

Complete list of Γ -point frequencies of the α and the β phase at zero pressure is provided in Table 3 together with their symmetry and optical activity. In case of the α phase, the frequencies are compared with experimental IR and Raman data from literature and overall good agreement is reached in line with our previous findings.¹ In both AgF_2 phases, the Raman and IR frequencies increase monotonically and quite linearly with pressure in the entire pressure ranges considered within this study as shown in Figure 6. The only two exceptions are the lowest energy IR-active B_{2u} mode in α and Raman-active E_g mode in the β phase. The latter slightly softens above 6 GPa, but the structure remains dynamically stable even at 20 GPa. This contrasts with the situation in the α phase, where the lowest-energy B_{2u} mode becomes dynamically unstable at 6 GPa (witnessed by negative energy values in Figure 6). Softening of this mode was used to explain the phase transition from the orthorhombic Pbca to the high-pressure $\text{Pca}2_1$ structure in the α phase.⁸

3.4 Phase diagram and thermodynamic stability

The comparison of the static energy dependence on volume and correction to vibrational zero-point energies (ZPE) is shown for both AgF_2 phases in left panel of Figure 2. The static energy minima are well distinguished and they have similar energy dependence on volume, while β has higher ground state energy than α at all calculated pressures. At zero pressure the difference amounts to 0.146 eV/ AgF_2 , which is close to the previously calculated DFT+U value of 0.17 eV/ AgF_2 .⁶ Calculated ZPEs per one AgF_2 unit are also strikingly similar within the pressure range studied; they amount to 0.125 eV and 0.122 eV per one AgF_2 unit for α and β , respectively. Thus, inclusion of the ZPE to the internal energy does not affect the relative stability of both forms. The calculated ground state thermodynamic data are summarized in Table 4.

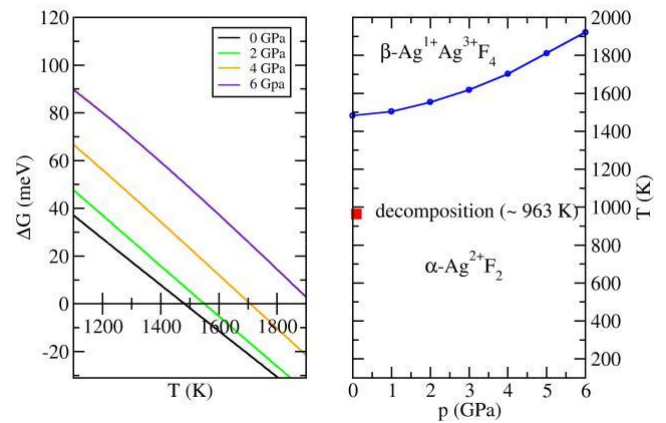


Fig. 7 The Gibbs energy isobars of thermodynamic equilibrium between the α and the β AgF_2 phase in the temperature range 1500–1900 K (left) and α - β phase diagram (right).

Impact of temperature on relative thermodynamic stability of the α and β phase is illustrated in Figure 7. The left panel shows relative Gibbs energy differences between α and β in function of temperature at constant pressure. The Gibbs energy isobars were evaluated at five pressure points within the region 0–8 GPa. They represent thermodynamic equilibria between α and β at constant pressure. The phase boundary between α and β was determined from sections of the isobar with the x-axis of the diagram. The obtained α - β phase diagram is visualized for the pressure range 0–6 GPa and temperature range 1500–1900 K in left panel of Figure 7. These calculations indicate that α is the thermodynamically stable phase in a broad field of temperature and pressure. β becomes thermodynamically preferred only at very high temperature, which additionally increases with pressure. At zero pressure, stability field of β over α extends above 1500 K, which, however, substantially exceeds the experimentally determined value of thermal decomposition temperature of the latter (963 K).⁴¹ The fact that the β phase was observed in experiments at ambient conditions suggests that it is metastable with respect to a form at lower temperatures. This is in accordance with its

Table 3 Calculated G-point frequencies of the α - and β -AgF₂. In case of a, available experimental data are included. Symmetry and optical activity (in brackets) of the normal modes is shown: IR – infrared active, R – Raman active, w – weak, sh – shoulder, m – medium intensity peak.

a								b							
#	Irr	f/cm ⁻¹	#	Irr	f/cm ⁻¹	#	Irr	f/cm ⁻¹	#	Irr	f/cm ⁻¹	#	Irr	f/cm ⁻¹	
		Exp ¹	DFT+U		Exp ¹	DFT+U		DFT+U		DFT+U			DFT+U		
1	B2u (IR)		24	18	Ag (R)	232-233	222	1	Eg (R)	53	18	Eu (IR)	248		
2	Ag (R)	57	62	19	B3g (R)	244	246	2	B1u	61	19	A1g (R)	436		
3	Au		73	20	B2g (R)	258	250	3	A2g	80	20	Eg (R)	447		
4	B1u (IR)	93w	90	21	B1g (R)	290-291	293	4	Eu (IR)	96	21	B2g (R)	448		
5	B3u (IR)	93w	93	22	Ag (R)	311-312	307	5	B1g (R)	101	22	Eu (IR)	529		
6	Au		98	23	B1u (IR)	307m	309	6	Eg (R)	105	23	B1u	533		
7	B1g (R)	102-117	115	24	B2u (IR)	307m	310	7	Eu (IR)	111	24	A2u (IR)	538		
8	B3g (R)	125	127	25	Au		321	8	A2u (IR)	129					
9	B2u (IR)	139sh	134	26	B1g (R)	337	326	9	B2u	136					
10	B1u (IR)		138	27	B3u (IR)	341sh	347	10	Eg (R)	140					
11	B3u (IR)	159w	154	28	B3u (IR)	441vs	441	11	A2u (IR)	201					
12	Au		161	29	B3g (R)		442	12	Eu (IR)	212					
13	B3u	168m	164	30	B2g (R)	446	443	13	A2g	214					
14	B2g (R)	162-174	172	31	B1u (IR)		453	14	A1g (R)	220					
15	Au		183	32	B2u (IR)		455	15	B2g (R)	223					
16	B1u (IR)	193m	185	33	Au		462	16	A1u	226					
17	B2u (IR)	193m	186					17	B1u	241					

Table 4 Ground-state energies (EGS), zero-point energies (ZPE), relative ground state and free energies (ΔE_{GS} , ΔE_{Free}), the volumes per one AgF₂ unit (V), bulk moduli (B₀) and their pressure derivatives (B'₀) calculated for α - and β -AgF₂ at p, T = 0. B₀ and B'₀ were fitted to Birch-Murnaghan equation of state.⁴⁰ The energies are calculated per one AgF₂ unit.

	ΔE_{GS}	E_{GS}	ZPE	ΔE_{Free}	V	B ₀	B' ₀
	(eV)	(eV)	(eV)	(eV)	(Å ³)	(GPa)	(GPa)
a	0	-9.392	0.125	0	40.46	50	8.38
b	0.146	-9.248	0.122	0.141	40.83	54	5.84

dynamic (phonon) stability as computed here (Figure 5, bottom). Moreover, the experimentally observed mild exoergonic transformation to the α phase¹⁰ agrees with the relative energies of both phases derived here from the first principles (0.14 eV corresponds to 13.5 kJ/mol).

3.5 Comparison of β -AgF₂ with NaCuO₂ and AgO

One can compare β -AgF₂ and oxocuprate NaCuO₂, which has been studied as reference compound for the existence of Cu³⁺ species in high-T oxocuprate superconductors.^{14–16} Both compounds contain formally d⁸ cation (Ag³⁺ or Cu³⁺) in square planar coordination with the ligands (respective building units are [Ag³⁺F₄] or [Cu³⁺O₄] plaquettes) and are diamagnetic insulators with the metal Cu³⁺/Ag³⁺ states positioned at lower energies relative to the p states of ligands. The insulating band gap of NaCuO₂ was measured by photoemission spectroscopy to be 1 – 2 eV,¹⁵ which is comparable to bandgap of β from hybrid DFT (1.2 eV). The two compounds however differ in crystal structure and type of the counter cation that greatly define the details of electronic structure. The isolated [Ag³⁺F₄] plaquettes in β - AgF₂ are contrasted with infinite [Cu³⁺O₂] chains of edge-sharing [Cu³⁺O₄] plaquettes.⁴² Additionally, the valence and conduction bands in NaCuO₂ are constructed only from the Cu³⁺ d and O p states,¹⁶ while in case of β -AgF₂, the picture is additionally complicated by presence of the Ag¹⁺ d states just below the Fermi level (Figure 3, bottom). These additional states push the Ag³⁺

d and F p states further below the Fermi level in respect to the Cu³⁺ d and O p states in NaCuO₂.¹⁶ These differences account for distinct character of the band gap in both systems.

It is also instructive to compare β -AgF₂ with its oxygen counterpart Ag¹⁺Ag³⁺O₂. In this case the two compounds are truly isoelectronic with comparable hybrid DFT values of insulating bandgap (1 eV),^{22,23,43} which in the case of AgO agree very well with the experimental value of 1.0–1.1 eV.^{44,45} In the monoclinic AgO, the Ag³⁺ cations form two-dimensional infinite puckered layers of corner-sharing [Ag³⁺O₄] plaquettes.¹⁷ This contrasts the isolated [Ag³⁺F₄] plaquettes in β -AgF₂ but is reminiscent of the puckered layers in α -AgF₂. Concerning the electronic DOS, the highly localized character of the Ag¹⁺ and Ag³⁺ states in β - AgF₂ (Figure 3, bottom and S5 in ESI) is quite distinct also from the highly dispersed Ag¹⁺ and Ag³⁺ d states in AgO where they additionally strongly overlap with each other and O p states.²² Thus, charge disproportionation in β -AgF₂ is more pronounced relative to AgO.

4 Conclusions

Crystal and electronic structure, lattice dynamics and thermodynamic stability of little known mixed-valent diamagnetic Ag¹⁺Ag³⁺F₄ β form of AgF₂ was thoroughly examined for the first time and compared with well known antiferromagnetic Ag²⁺F α form within the framework of Density Functional Theory based methods, phonon direct method and quasiharmonic approximation. Results of a detailed analysis of lattice dynamics and impact of temperature on stability of the α phase were also for the first time presented. The modelled KBrF₄ type crystal structure of β is comparable to NaAgF₄ in line with well known similarities of Na⁺ and Ag⁺ cations, and its tetragonal c/a ratio fits ideally within the observed trend among the ternary metal fluorides M'MF₄ with coinage (M) and alkali metals (M'). Crystal structure of both, α and β , are structurally closely related and can be derived from the common fluorite parent prototype via distinct order parameter X5+ and L3 + /L3, respectively. Their volumes are also very close, the volume of β is only slightly larger

(1%), and both exhibit comparable compressibility ($B_0^\alpha = 50$ GPa and $B_0^\beta = 54$ GPa), which is simultaneously considerably higher than for their lighter copper counterpart CuF₂. Electronic structure calculations revealed highly localized Ag¹⁺ and Ag³⁺ states in β relative to highly dispersed Ag²⁺ ones in α . Both phases are insulators, the bandgap of β being by factor of 2 lower at all considered pressures, as revealed by DFT+U results (at zero pressure $E_{\text{gap}}^\alpha = 1.167$ eV and $E_{\text{gap}}^\beta = 0.61$ eV). The hybrid DFT bandgaps were computed to be by factor of 2 wider. Phonon densities of states reveal pronounced differences related to presence of distinct Ag species in each case. In α , the stretching and bending modes are highly coupled and the overall phonon bands are greatly dispersed. On the other hand, phonon structure of β is characteristic of highly localized bands, the symmetric and asymmetric [Ag³⁺F₄] vibrations are completely decoupled from each other as well as from the lower-energy bending and lattice modes. The considerably increased frequencies of the asymmetric [Ag³⁺F₄] modes relative to those of [Ag²⁺F₄], confirm presence of increased covalency of chemical bonds in β relative to α . In both phases, the IR and Raman active modes increase monotonically with pressure. The only exception is the lowest-energy IR active B_{2u} mode in α and the lowest-energy Raman E_g mode in β . It was shown that the former mediates the phase transition to ferroelectric Pca2₁ structure in α .⁸ On the other hand, the latter softens only slightly and β remains dynamically stable at all calculated pressures up to 20 GPa. The α phase is thermodynamically preferred over β also at high pressures and temperatures. β phase cannot be reached experimentally in close-to-equilibrium conditions with α : its calculated temperature stability region lies far above the thermal decomposition temperature of alpha phase in the p–T diagram. Computed results are in line with experimental observation: β phase may be obtained exclusively as a metastable species when starting from Ag¹⁺ and Ag³⁺F₄ precursors.⁴¹ Finally, the insulating hybrid DFT bandgap of β is comparable with bandgaps of related mixed-valent Na¹⁺Ag³⁺O₂ and Ag¹⁺Ag³⁺O₂, and electronic disproportionation is more pronounced in β -AgF₂ relative to AgO.

Acknowledgements

K.T. and M.D. acknowledge the European Regional Development Fund, Research and Innovation Operational Program (project No. ITMS2014+: 313011W085), the Slovak Research and Development Agency (grant No. APVV-18-0168) and Scientific Grant Agency of the Slovak Republic (grant No. VG 1/0223/19). WG acknowledges the Polish National Science Center (NCN) for the Beethoven project (2016/23/G/ST5/04320). The research was carried out using machines of the Interdisciplinary Centre for Mathematical and Computational Modelling (ICM), University of Warsaw under grant ADVANCE++ (no. GA76-19) and Aurel supercomputing infrastructure in CC of Slovak Academy of Sciences acquired in projects ITMS 26230120002 and 26210120002 funded by ERDF.

Notes and references

- 1 J. Gawraczynski, D. Kurzydłowski, W. Gadomski, Z. Mazej, T. Jaron, A. Ozarowski, S. Hill, P. J. Leszczynski, K. Tokár, P. Derzsi, M. Barone, K. L. J. Wohlfeld and G. W., *PNAS*, 2019, **116**, 1295–1500.
- 2 P. Fischer, D. Schwarzenbach and H. M. Rietveld, *J. Phys. Chem. Solids*, 1971, **32**, 543–550.
- 3 P. Fischer, G. Roullet and D. Schwarzenbach, *J. Phys. Chem. Solids*, 1971, **32**, 1641–1647.
- 4 D. Kurzydłowski, M. Derzsi, P. Barone, A. Grzelak, V. Struzhkin, J. Lorenzana and W. Grochala, *Chem. Commun.*, 2018, **54**, 10252–10255.
- 5 *Photonic and Electronic Properties of Fluoride Materials*, ed. A. Tressaud and P. K., Elsevier Inc., Radarweg 29, PO Box 211, 1000 AE Amsterdam, Netherlands The Boulevard, Langford Lane, Kidlington, Oxford OX5 1GB, UK 50 Hampshire Street, 5th Floor, Cambridge, MA 02139, USA, 2016.
- 6 J. Romiszewski, W. Grochala and L. Stolarczyk, *J. Physics: Condensed Matter*, 2007, **19**, 116206.
- 7 T. Jaron and W. Grochala, *Phys. Stat. Sol. (RRL)*, 2008, **2**, 71–73.
- 8 A. Grzelak, J. Gawraczynski, T. Jaron, D. Kurzydłowski, A. Budzianowski, Z. Mazej, P. J. Leszczynski, V. B. Prakapenka, M. Derzsi, V. Struzhkin and W. Grochala, *Inorg. Chem.*, 2017, **56**, 14651–14661.
- 9 A. Grzelak, J. Gawraczynski, T. Jaron, D. Kurzydłowski, Z. Mazej, P. J. Leszczynski, V. B. Prakapenka, M. Derzsi, V. Struzhkin and W. Grochala, *Dalton. Trans.*, 2017, **46**, 14742–14745.
- 10 C. Shen, B. Zemva, G. M. Lucier, O. Graudejus, J. A. Allman and N. Bartlett, *Inorg. Chem.*, 1999, **38**, 4570–4577.
- 11 B. G. Muller, *Angew. Chem. Int. Ed. Engl.*, 1987, **26**, 1081–1097.
- 12 O. Graudejus, A. P. Wilkinson and N. Bartlett, *Inorg. Chem.*, 2000, **39**, 1545–1548.
- 13 A. S. Moskvin, *Phys. Rev. B*, 2011, **84**, 075116.
- 14 T. Mizokawa, H. Namatame, A. Fujimori, K. Akeyama, H. Kon-doh, H. Kuroda and N. Kosugi, *Phys. Rev. Lett.*, 1991, **67**, 1638–1641.
- 15 T. Mizokawa, A. Fujimori, H. Namatame, K. H. Akeyama and N. Kosugi, *Phys. Rev. B*, 1994, **49**, 7193–7204.
- 16 S. Nimkar, N. Shanthi and D. D. Sarma, *Proc. Indian Acad. Sci. (Chem. Sci.)*, 1994, **106**, 393–405.
- 17 J. A. Mcmillan, *J. Inorg. Nucl. Chem.*, 1960, **13**, 28–31.
- 18 K. Yvon, A. Bezinge, P. Tissot and P. Fischer, *J. Solid State Chem.*, 1986, **65**, 225–230.
- 19 P. Behrens, S. U. Aßmann, Bilow, C. Linke and M. Jansen, *Z. anorg. allg. Chem.*, 1999, **625**, 111–116.
- 20 P. M. Biemann, M. and Schwaller, P. Ruffieux, O. Gröning, L. Schlapbach and P. Gröning, *Phys. Rev. B*, 2002, **65**, 235431–1–5.
- 21 D. Tudela, *Journal of Chemical Education*, 2008, **85**, 161103(R).

- 22 J. P. Allen, D. O. Scanlon and G. W. Watson, *Phys. Rev. B*, 2010, **81**, 863–865.
- 23 A. Grzelak, J. Gawraczynski, T. Jaron, M. Somayazulu, M. Derzsi, V. Struzhkin and W. Grochala, *Inorg. Chem.*, 2017, **56**, 5804–5812.
- 24 A. J. Garza and G. E. Scuseria, *J. Phys. Chem. Lett.*, 2017, **7**, 41654170.
- 25 G. Kresse and J. Furthmüller, *Phys. Rev.*, 1996, **54**, 11169.
- 26 G. Kresse and D. Joubert, *Phys. Rev.*, 1996, **59**, 1758.
- 27 G. I. Csonka, J. P. Perdew, A. Ruzsinszky, P. H. T. Philipsen, S. Lebégue, J. Paier, O. A. Vydrov and J. G. Ángyán, *Phys. Rev. B*, 2009, **79**, 155107.
- 28 A. I. Liechtenstein, V. I. Anisimov and J. Zaanen, *Phys. Rev. B*, 1995, **52**, R5467(R).
- 29 A. V. Krukau, O. A. Vydrov, A. F. Izmaylov and G. E. Scuseria, *J. Chem. Phys.*, 2006, **125**, 224106.
- 30 H. Monkhorst and J. Pack, *Phys. Rev. B*, 1976, **13**, 5188.
- 31 A. Togo and I. Tanaka, *Scr. Mater.*, 2015, **108**, 1–5.
- 32 R. Hoppe and R. Homann, *Zeitschrift fuer Anorganische und Allgemeine Chemie*, 1970, **379**, 193–198.
- 33 O. Graudejus, A. Wilkinson and N. Bartlett, *Inorg. Chem.*, 2000, **39**, 1545–1548.
- 34 G. Jones and A. Edwards, *Journal of the Chemical Society A: Inorganic, Physical, Theoretical (1966-1971)*, 1969, **1969**, 1936–1938.
- 35 R. Shannon, *Acta Cryst. A*, 1976, **32**, 751–767.
- 36 H. T. Stokes, D. M. Hatch and B. J. Campbell, <https://stokes.byu.edu/iso/isotropy.php>.
- 37 D. Kurzydłowski, *Crystals*, 2018, **8**, 140(pp13).
- 38 V. T. Fleischer and R. Hopper, *Z. anorg. allg. Chem.*, 1982, **492**, 76–82.
- 39 V. R.-H. Odenthal and R. Hopper, *Z. anorg. allg. Chem.*, 1971, **385**, 72–101.
- 40 F. Birch, *J. Geophys. Res.*, 1978, **83**, 1257–1268.
- 41 W. Grochala, *Journal of Fluorine Chemistry*, 2008, **129**, 82–90.
- 42 P. J., W. Paulus, M. Schmalz and R. Schöllhorn, *J. Solid State Chem.*, 1990, **89**, 308–314.
- 43 I. Włodarska, M. Derzsi and W. Grochala, *Phys. Status Solidi RRL*, 2015, **9**, 401–404.
- 44 B. E. Breyfogle, C. J. Hung, M. G. Shumsky and J. A. Switzer, *J. Electrochem. Soc.*, 1996, **143**, 2741–2746.
- 45 N. Ravi Chandra Raju, K. Jagadeesh Kumar and A. Subrahmanyam, *J. Phys. D: Appl. Phys.*, 2009, **42**, 135411(6pp).

Supporting Material (ESI) to

Comparative computational study of antiferromagnetic and mixed-valent diamagnetic phase of AgF₂: crystal, electronic and phonon structure and p-T phase diagram

Kamil Tokár,^{a;b} Mariana Derzsi,^{a;c} and Wojciech Grochala^c

^a*Advanced Technologies Research Institute, Faculty of Materials Science and Technology in Trnava, Slovak University of Technology in Bratislava, J. Bottu 25, 917 24 Trnava, Slovakia.*

E-mail: mariana.derzsi@stuba.sk

^b*Institute of Physics, Slovak Academy of Sciences, Dúbravská cesta 9, 845 11 Bratislava, Slovakia.*

^c*Center of New Technologies, University of Warsaw, Żwirki i Wigury 93, 02089 Warsaw, Poland.*

Table S1. Comparison of α -AgF₂ and β -AgF₂ lattice parameters with function of pressure. DFT+U results.

P (GPa)	α -AgF ₂			β -AgF ₂	
	a(Å)	b (Å)	c(Å)	a (Å)	c (Å)
0	5.498	5.824	5.055	5.524	10.704
2	5.466	5.730	5.005	5.449	10.653
4	5.445	5.650	4.965	5.387	10.610
6	5.4285	5.610	4.900	5.332	10.575
8	5.420	5.570	4.844	5.286	10.543
10	NA	NA	NA	5.244	10.517
20	NA	NA	NA	5.077	10.423

Fig S1. Electronic density of states for α -AgF₂ (top) and β -AgF₂ phase (bottom) at 0 GPa. The Fermi level is set to 0 eV. **Hybrid DFT** results.

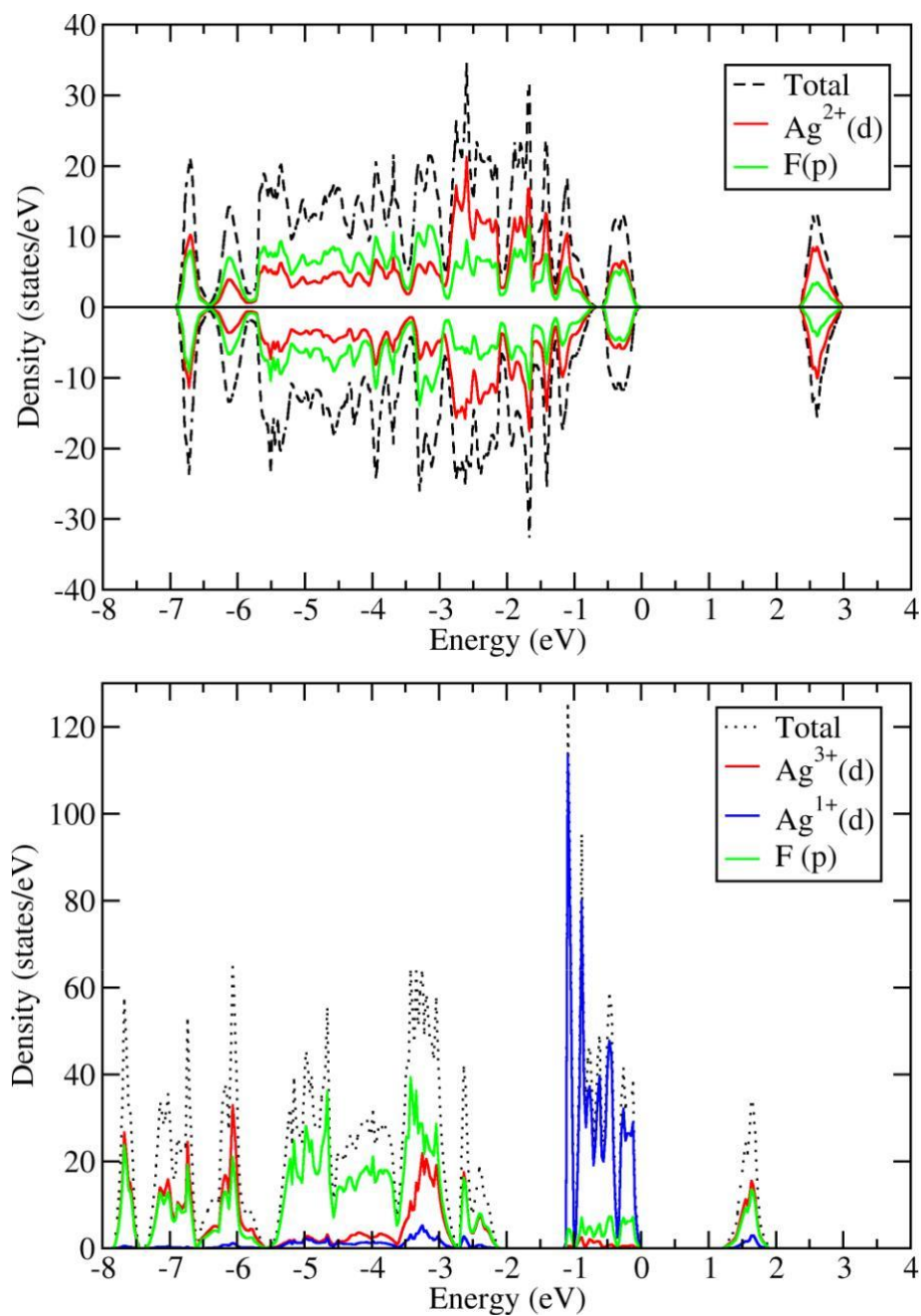


Fig S2. Electronic density of states for α -AgF₂ phase in pressure range 0 - 6 Gpa. The Fermi level is set to 0 eV. **DFT+U** results.

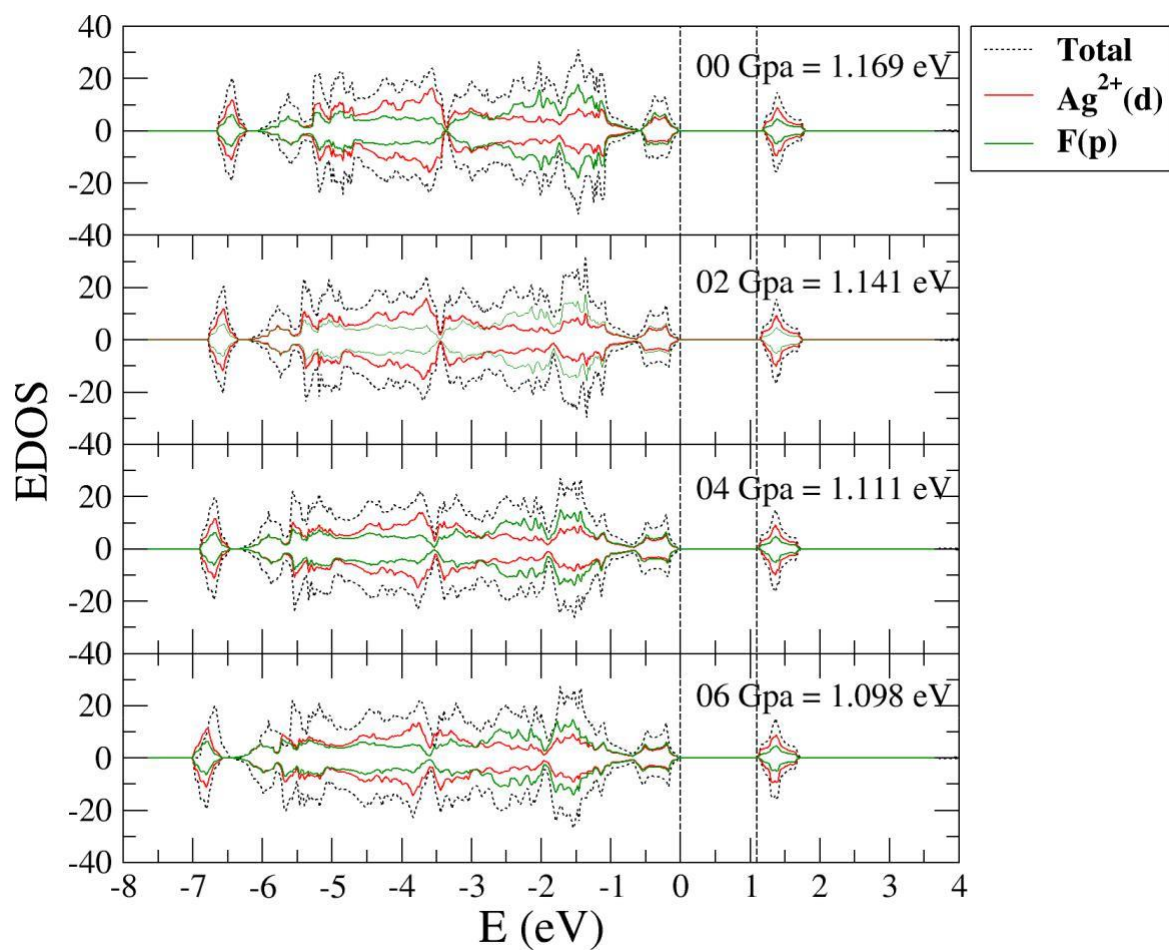


Fig S3. Electronic density of states for β -AgF₂ phase in pressure range 0 - 6 Gpa. The Fermi level is set to 0 eV. **DFT +U** results.

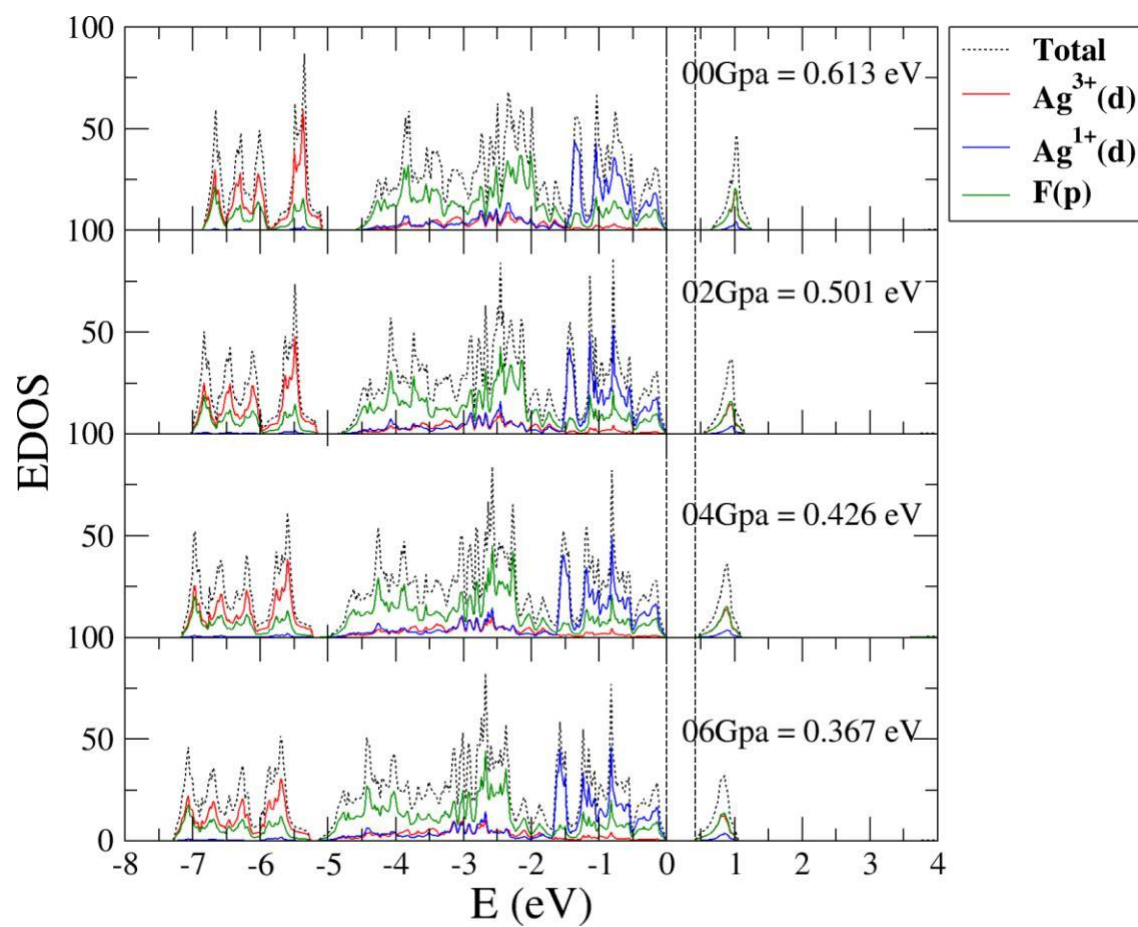


Fig S4. Electronic density of states for α -AgF₂ phase in pressure range 0 - 6 Gpa. The Fermi level is set to 0 eV. **Hybrid DFT** results.

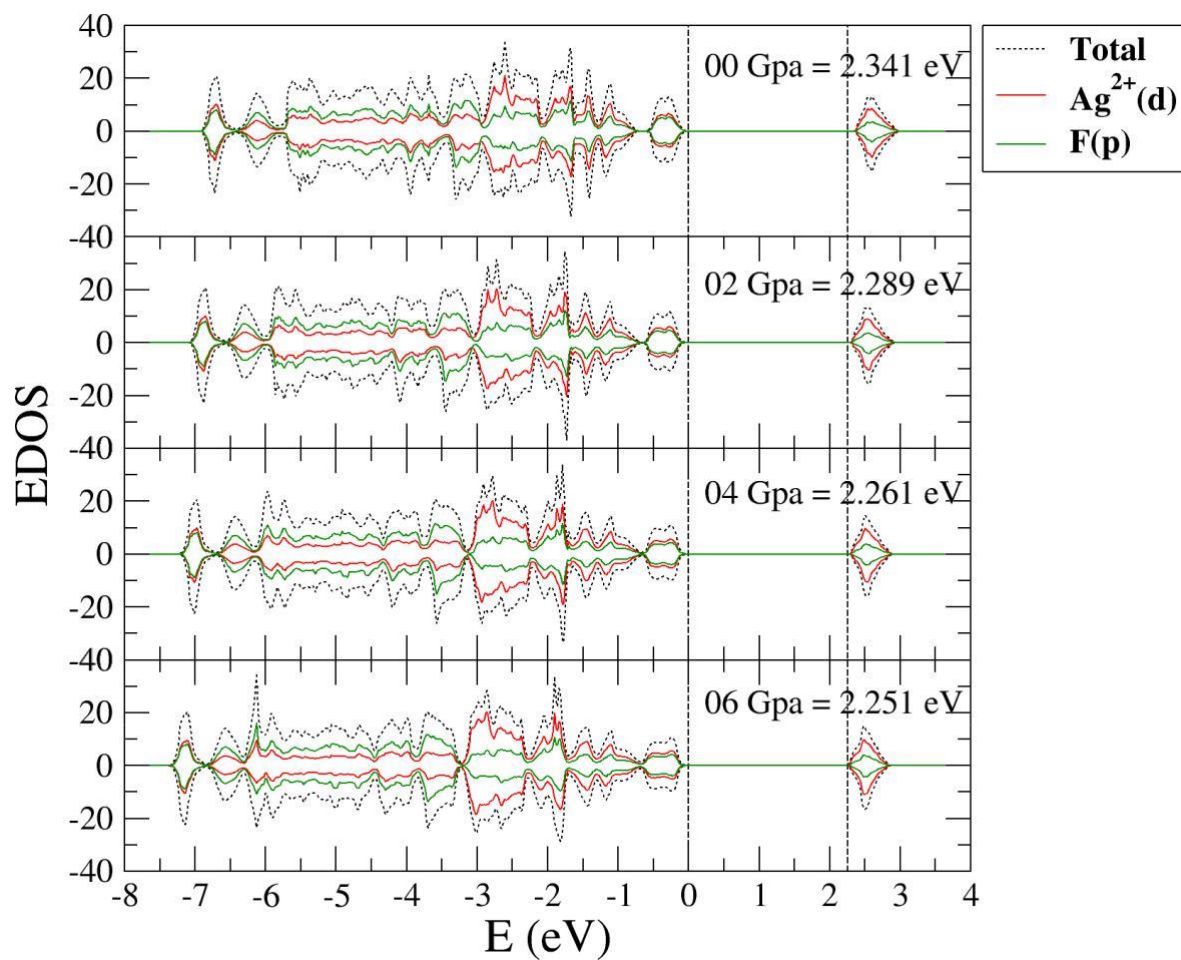


Fig S5. Electronic density of states for β -AgF₂ phase in pressure range 0 - 6 Gpa. The Fermi level is set to 0 eV. **Hybrid DFT** results.

